



**HAL**  
open science

# Numerical Modelling of the Nonlinear Shear Creep Behavior of FRP-Concrete Bonded Joints

François Soleilhet, Marc Quiertant, Karim Benzarti

► **To cite this version:**

François Soleilhet, Marc Quiertant, Karim Benzarti. Numerical Modelling of the Nonlinear Shear Creep Behavior of FRP-Concrete Bonded Joints. *Materials*, 2023, 16 (2), 15 p. 10.3390/ma16020801 . hal-03939124

**HAL Id: hal-03939124**

**<https://hal-enpc.archives-ouvertes.fr/hal-03939124>**

Submitted on 14 Jan 2023

**HAL** is a multi-disciplinary open access archive for the deposit and dissemination of scientific research documents, whether they are published or not. The documents may come from teaching and research institutions in France or abroad, or from public or private research centers.

L'archive ouverte pluridisciplinaire **HAL**, est destinée au dépôt et à la diffusion de documents scientifiques de niveau recherche, publiés ou non, émanant des établissements d'enseignement et de recherche français ou étrangers, des laboratoires publics ou privés.



Distributed under a Creative Commons Attribution| 4.0 International License



*materials*

IMPACT  
FACTOR  
**3.748**

Indexed in:  
**PubMed**

Article

---

# Numerical Modelling of the Nonlinear Shear Creep Behavior of FRP-Concrete Bonded Joints

---

François Soleilhet, Marc Quiertant and Karim Benzarti

**Special Issue**

Internal and External FRP Reinforcement of Civil Engineering Structures

Edited by




Dr. Sylvain Chataigner, Dr. Karim Benzarti and Dr. Marc Quiertant



<https://doi.org/10.3390/ma16020801>

## Article

# Numerical Modelling of the Nonlinear Shear Creep Behavior of FRP-Concrete Bonded Joints

François Soleilhet <sup>1</sup>, Marc Quiertant <sup>2,†</sup> and Karim Benzarti <sup>3,\*,†</sup><sup>1</sup> EDF Lab Les Renardières, F-77250 Moret-Loing-et-Orvanne, France<sup>2</sup> Matériaux et Structures (MAST) Department, Expérimentation et Modélisation pour le Génie Civil et Urbain (EMGCU), University Gustave Eiffel, F-77447 Marne-la-Vallée, France<sup>3</sup> Lab Navier, University Gustave Eiffel, Ecole Nationale des Ponts et Chaussées (ENPC), Centre National de la Recherche Scientifique (CNRS), F-77447 Marne la Vallée, France

\* Correspondence: karim.benzarti@univ-eiffel.fr

† These authors contributed equally to this work.

**Abstract:** This paper presents a numerical investigation of the shear creep behavior of the adhesive joint in concrete structures strengthened by externally bonded fibre-reinforced polymers (FRP) composites. Based on experimental data collected in a previous study, creep constitutive equations were developed for the adhesive layer and implemented into a finite element code. The proposed model extends the classical one-dimensional formulation of Burgers creep model to a fully 3D model and introduces the nonlinearity of the model parameters. This numerical approach was first used to simulate the nonlinear creep behavior of bulk epoxy samples; it was then extended to predict the nonlinear creep response of the FRP-concrete interface in double lap shear specimens. Globally, a fair agreement was obtained between numerical results and experimental evidences. As a main result, it was found that creep induces a redistribution of the interfacial shear stress along the FRP-concrete lap joint, leading both to a stress relaxation near the loaded end of the adhesive joint and to an increase in the effective transfer length.

**Keywords:** epoxy adhesive; FRP-concrete bonded joints; nonlinear creep; finite element modelling



**Citation:** Soleilhet, F.; Quiertant, M.; Benzarti, K. Numerical Modelling of the Nonlinear Shear Creep Behavior of FRP-Concrete Bonded Joints.

*Materials* **2023**, *16*, 801.

<https://doi.org/10.3390/ma16020801>

Academic Editors: Angelo Marcello Tarantino and Carlos Leiva

Received: 23 November 2022

Revised: 13 December 2022

Accepted: 9 January 2023

Published: 13 January 2023



**Copyright:** © 2023 by the authors. Licensee MDPI, Basel, Switzerland. This article is an open access article distributed under the terms and conditions of the Creative Commons Attribution (CC BY) license (<https://creativecommons.org/licenses/by/4.0/>).

## 1. Introduction

Externally Bonded (EB) Fiber Reinforced Polymer (FRP) strengthening systems have been widely adopted for the rehabilitation of Reinforced Concrete (RC) structures since the late 1990's. The effectiveness of this retrofitting method has been clearly demonstrated in the literature [1–6] and several well-established international design guidelines are now available to practitioners with a view to ensuring proper field implementation [7–12]. In EB-FRP applications, service loads are transferred from the concrete structure to the FRP reinforcement through the adhesive joint, which deforms mainly under shear stress. Due to its inherent viscoelastic nature, the polymer adhesive layer may exhibit substantial creep deformation when subjected to sustained shear load, hence affecting the stress transfer process between the host structure and the FRP material [13–16]. This creep effect is possibly emphasized by the evolution of the adhesive properties (loss of stiffness) due to environmental ageing under service conditions [17,18]. In this context, the long-term performance of the structural retrofit strongly relies on the delayed behavior of the adhesive joint. Therefore, knowledge of the time dependent response of the bulk polymer adhesive and the FRP-concrete adhesive bond under creep load is of great importance for safety issues and for optimizing the maintenance strategy as well. It becomes even crucial in the case of prestressed FRP systems, where delayed viscous effects of the adhesive bond may result in critical prestress losses [19,20].

The viscoelastic response of bulk polymer materials has been widely investigated in the literature, through both experimental studies and theoretical approaches. Experimental

works rely most often on tensile tests at constant load levels [16,21–23] although few authors have developed specific setups to investigate the creep behavior of bulk polymers subjected to sustained shear loading [24]. Differently, the creep behavior of the adhesive joints in FRP-concrete assemblies is less documented. In general, it is admitted that adhesive joints behave differently from the bulk polymer material, as they are subjected to complex stress fields [25,26]. For this reason, the creep response of the adhesive layer is often directly investigated by performing shear tests on FRP-concrete assemblies [13,27,28]. Nevertheless, several researchers have shown that the delayed response of FRP-concrete specimens can still be accurately described by identifying in a first stage the creep behavior law of the bulk adhesive, and then introducing this law into a finite element (FE) model of the FRP-concrete assembly. For instance, Zehsaz et al. [29] carried out uniaxial tensile creep tests on bulk epoxy samples, which allowed them to identify the parameters of a rheological model derived from Maxwell and Zener's model [29]. This model was then used to predict the creep response of double shear joints using the FE method, and numerical results showed good agreement with experimental data. A similar approach was adopted by Houhou et al. [17]. These authors performed short-term tensile creep tests on bulk adhesive samples at several temperatures and at different stress levels, and they used these experimental data to build the creep compliance master curve according to the time-temperature superposition principle (TTSP). A rheological Burgers model was then calibrated from this master curve, which allowed to describe the nonlinear creep response of the bulk adhesive. Finally, this behavior law was successfully implemented in a FE model to predict the creep response of FRP-concrete bonded assemblies. Besides, Houachine et al. [16] proposed an analytical model to describe the long-term load-bearing capacity of concrete beams strengthened with EB-FRPs, which includes the creep contributions of all component materials (i.e., concrete, adhesive and FRP). A combined cohesive-bridging zone model was then proposed to model both the crack-processing zone near the interface (cohesive zone model) and the particle-interlocking region (bridging zone model). To predict the long-term response of the FRP-concrete interface, the fracture energy was kept constant in each zone and at each step of the calculation. After calibration of the bond-slip model with experimental results from the literature describing the instantaneous response of the FRP-concrete interface, long-term simulations were compared to those of Houhou et al. [17], showing good agreement.

Hadjazi et al. [30] also studied the long-term behavior of RC beams strengthened by EB-FRPs, but with a particular focus on the time evolution of shear stresses induced by flexural cracks along the adhesive joint. In continuity with previous works [16,31], these authors considered the creep behaviors of all the component materials of the retrofitted beam to develop an original viscoelastic model, in which the influence of environmental conditions are introduced through adjusted creep factors depending on the relative humidity. It is noteworthy that Eurocode 2 [32] suggests the construction of a creep function based on the creep behavior laws of all component materials of the bonded assembly (concrete, adhesive and FRP). Following a cohesive zone model approach and considering the total energy constant, the approach of Hadjazi et al. [30] was found effective to analyze the creep response of a FRP-plated RC beam, including the debonding stage of the FRP plate. In most studies from the literature, unidimensional formulations of the rheological creep models are proposed. This approach is relevant for many strengthening configurations using FRPs, like flexural strengthening of longitudinal beams, where the predominant load in the bonded FRP reinforcement is uniaxial tension. It has also proven to be effective in several FE analysis [33]. However, 1-D formulation is less appropriate in the case of structures with complex geometries, where non-planar bonding surfaces are submitted to 2-D or 3-D stress fields [34].

In this study, a simple fully 3-D formulation of the creep behavior of the adhesive layer is proposed, that considers the stress-dependency of model parameters. The main originality of this approach lies in the proposal of a multi-axial creep model developed in a 3D tensor formalism. In this framework, the nonlinearity of the adhesive creep is managed by correlating the model parameters with the mechanical stress state of the polymer

material. This approach could also be enriched at a further stage by taking into account the dependency of the adhesive creep upon hygro-thermal conditions. A second originality of the model is the use of the constitutive law generator MFront, which allows a portability of the behavior law between different FE codes (ABAQUS, CAST3M, Code\_Aster,...) without further development. The proposed model is then used to predict the creep behavior of double shear specimens, and the numerical results obtained are compared to those previously obtained by Houhou et al. [17] for the same test configuration [17,35].

## 2. Nonlinear Creep Model

When an FRP retrofitted RC structure is exposed to sustained load, concrete creep occurs in the compression zone, FRP laminates are subjected to tensile creep and the adhesive joint is rather subjected to shear creep. In this paper, we will focus on the creep behavior of the adhesive layer, as this latter is considered to bring the highest contribution to the delayed response of the overall assembly near the loaded end of the adhesive joint. Moreover, in actual repair works, the RC beam has generally been subjected to sustained load for a long period before application of the FRP strengthening system and, thus, concrete and steel have already experienced significant part of their creep strains. However, the proposed model could be applied (after adequate calibration) to all the component materials of the FRP-strengthened RC structure. In the following section, the key characteristics of the adhesive joint are discussed. As proposed in [35], an uncracked concrete substrate is considered in order to simplify the analysis and highlight the global effects of the adhesive creep.

Although creep of polymers is known to be dependent on time, stress, and environmental conditions [36], the proposed modelling of the time-dependent strain in a viscoelastic 3D framework is developed accounting for material nonlinearities and stress state dependency, but it will not take into consideration the effects of temperature and relative humidity. Therefore, the application of this model is restricted to an isothermal condition in the temperature range below the glass transition temperature ( $T_g$ ) of the polymer adhesive.

### 2.1. Constitutive Equations

For the sake of clarity, the one-dimensional Burgers material, which is the base of the present model, is depicted (Figure 1). However, all the following equations are developed in a three-dimensional framework. Burgers material is composed of three main blocks organized in series: an elastic material (a Hookean spring exhibiting a modulus of elasticity  $E_k$ ), followed by a Kelvin–Voigt solid (with modulus of elasticity  $E_{kv}$  of the spring and viscosity  $\eta_{kv}$  of the dashpot), which is finally connected to a linear dashpot ( $\eta_{dash}$ ).

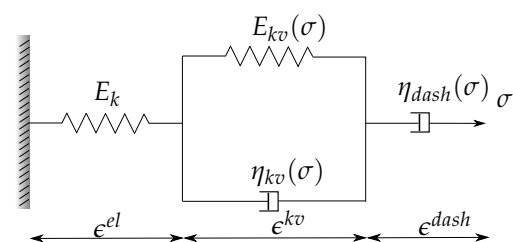


Figure 1. 1D schematic representation of Burgers material.

Therefore, the total strain rate is decomposed into three terms:

$$\dot{\epsilon}^{to} = \dot{\epsilon}^{el} + \dot{\epsilon}^{kv} + \dot{\epsilon}^{dash} \quad (1)$$

where the dot on top of strain stands for time derivative.  $\epsilon$ ,  $\epsilon^{el}$ ,  $\epsilon^{kv}$  and  $\epsilon^{dash}$  are, respectively, the tensors of the total, the elastic, the delayed elastic strain of the Kelvin–Voigt solid and the viscous strain of the Maxwell dashpot.

### 2.1.1. Elastic and Viscous Strains

From Equation (1) it can be concluded that the rate of total strain ( $\dot{\epsilon}$ ) is divided into an elastic part ( $\dot{\epsilon}^{el}$ ) and a viscous part ( $\dot{\epsilon}^v$ ).

$$\dot{\epsilon}^{to} = \dot{\epsilon}^{el} + \dot{\epsilon}^v \quad (2)$$

The elastic part of the strain rate, corresponding to instantaneous strain response, is given by Hooke's law:

$$\dot{\epsilon}^{el} = q_k \mathbb{C}_v : \dot{\sigma} \quad (3)$$

where ":" stands for double dot product,  $q_k$  ( $\text{Pa}^{-1}$ ) the elastic compliance ( $q_k = 1/E_k$  with  $E_k$  (Pa) the elastic stiffness) and  $\mathbb{C}_v$  the unit tensor of elastic compliance (fourth order tensor which is defined in Appendix A (written in Voigt notation)).

The evolution of the viscous part of the strain ( $\dot{\epsilon}^v$ ) is the sum of the strain evolution of the Kelvin–Voigt material described by a second order equation (Equation (4b)) and the evolution of the strain in the dashpot governed by Equation (4c). Thus, the three equations below govern the evolution of the model viscous part.

$$\dot{\epsilon}^v = \dot{\epsilon}^{kv} + \dot{\epsilon}^{dash} \quad (4a)$$

$$\tau_{kv} \dot{\epsilon}_v^{kv} + \epsilon_v^{kv} = q_{kv}(\sigma) \mathbb{C}_v : \sigma \quad \text{with} \quad q_{kv}(\sigma) = \frac{1}{E_{kv}(\sigma)} \quad (4b)$$

$$\dot{\epsilon}^{dash} = q_{dash}(\sigma) \mathbb{C}_v : \sigma \quad \text{with} \quad q_{dash}(\sigma) = \frac{1}{\eta_{dash}(\sigma)} \quad (4c)$$

where  $q_{kv}$  ( $\text{Pa}^{-1}$ ) and  $E_{kv}$  (Pa) are, respectively, the creep compliance and elastic modulus of the Kelvin–Voigt unit,  $\tau_{kv}$  (s) the retardation time equal to  $\eta_{kv}/E_{kv}$ ,  $q_{dash}$  ( $\text{Pa}^{-1}$ ) and  $\eta_{dash}$  (Pa s) the creep compliance and the dynamic viscosity associated to the linear dashpot part. The creep Poisson's ratio of the polymer is considered constant over time [37,38] and it is taken equal to the elastic Poisson's ratio ( $\nu$ ) due to the lack of information regarding transverse strain. Thus, the relaxation modulus in the shear direction ( $G_{kv}$ ) can be calculated from the relaxation modulus in axial direction ( $E_{kv}$ ) according to Equation (5).

$$G_{kv} = \frac{E_{kv}}{2(1 + \nu)} \quad (5)$$

### 2.1.2. Nonlinearity

Experimental evidences from the literature [17,39,40] have demonstrated the nonlinearity of the adhesive creep behavior. To manage this stress dependency, model parameters such as Kelvin–Voigt solid's stiffness and dynamic viscosity parameters ( $\eta_{dash}$  and  $\eta_{kv}$ ) are considered dependent upon applied stress ( $\sigma$ ). As suggested by Majda and Skrodzewicz [41], the nonlinearities are introduced by exponential function (Equations (6a) and (6b)).

$$E_{kv}(\bar{\sigma}) = E_{kv}^0 \exp(a_{kv} \bar{\sigma}) \quad (6a)$$

$$\eta_i(\bar{\sigma}) = \eta_j^0 \exp(b_j \bar{\sigma}) \quad (6b)$$

with  $E_{kv}^0$  (Pa),  $\eta_j^0$  (Pa s), respectively, the initial stiffness and the initial dynamic viscosity,  $a_{kv}$  and  $b_j$  both in ( $\text{Pa}^{-1}$ ) two scalars to account for the material nonlinearities (the index  $j$  refers to  $kv$  or  $dash$  depending on the case), and finally  $\bar{\sigma}$  (Pa) is a scalar value called the effective stress. To determine the effective stress, a linear combination of shear ( $\sigma_e$ )

and hydrostatic ( $\sigma_m$ ) components of stress tensor (Equation (7)) is used as formulated by Dean [39]. This combination is an analogy to the Drucker–Prager yield criterion.

$$\begin{aligned}\bar{\sigma} &= \frac{(\alpha + 1)}{2\alpha}\sigma_e + \frac{3(\alpha - 1)}{2\alpha}\sigma_m \\ \sigma_e &= \left[ \frac{1}{2} \left[ (\sigma_I - \sigma_{II})^2 + (\sigma_{II} - \sigma_{III})^2 + (\sigma_I - \sigma_{III})^2 \right] \right]^{\frac{1}{2}} = \sqrt{3J_2} \\ \sigma_m &= \frac{1}{3}(\sigma_I + \sigma_{II} + \sigma_{III}) = \frac{I_1}{3}\end{aligned}\quad (7)$$

with  $\sigma_I, \sigma_{II}, \sigma_{III}$  the principal stresses of the stress tensor,  $J_2$  the second principal invariant of the stress tensor and  $\alpha$  a scalar parameter. From Equation (7), it can be concluded that under a uniaxial tensile stress  $\sigma_t$ , the effective stress is equal to  $\sigma_t$ , while under a uniaxial compressive stress  $\sigma_c$ , the effective stress is equal to  $\sigma_c/\alpha$ . One should note that for low stress levels, the compliance curves obtained in tension or in compression look very similar. However, under higher stresses where material behaviors are expected to be nonlinear, differences may occur between tension and compression loadings (see for instance the study of Dean [39]). In this study, considering that there is no information regarding creep in compression for the experimental test modelled hereafter,  $\alpha$  is always assumed equal to 1. Nevertheless, it is possible to consider tension–compression asymmetry through this parameter.

## 2.2. Implementation

MFront constitutive law generator [42–44] available in the FE software Code\_Aster was used to implement the nonlinear creep model. Time integration was carried out using an implicit method based on a  $\theta$ -scheme.

### 2.2.1. Implicit Scheme

For the aforementioned  $\theta$ -scheme, the state variables to account for are the elastic strain  $\epsilon^e$  and the viscous strains  $\epsilon^{kv}$  and  $\epsilon^{dash}$ . The equations which govern the evolution of these state variables are determined from the increments of the different strains. To obtain these strain increments, time is subdivided into discrete instant  $t_i$  (with  $i = 1, \dots, n_{step}$ ) and the time increment is equal to  $\Delta t_i = t_{i+1} - t_i$ .

- The increment of total strain:

$$\Delta \epsilon_{i+1}^{to} = \Delta \epsilon_{i+1}^{el} + \Delta \epsilon_{i+1}^{kv} + \Delta \epsilon_{i+1}^{dash} = \Delta \epsilon_{i+1}^{el} + \Delta \epsilon_{i+1}^v \quad (8)$$

- The increment of elastic strain:

$$\Delta \epsilon_{i+1}^{el} = q_k \mathbb{C}_v : \Delta \sigma_{i+1} \quad \text{with} \quad q_k = \frac{1}{E_k} \quad (9)$$

- The increment of the two viscous strains:

$$\Delta \epsilon_{i+1}^{kv} = \frac{\Delta t}{\tau_{kv}} \left[ q_{kv} \mathbb{C}_v : \sigma_{i+1} - \epsilon_{i+1}^{kv} \right] \quad (10a)$$

$$\Delta \epsilon_{i+1}^{dash} = \frac{\Delta t}{\eta_{dash}} \mathbb{C}_v : \sigma_{i+1} \quad (10b)$$

For the resolution of these equations, the quantities  $\sigma_{i+1}, \epsilon_{i+1}^{kv}$  are evaluated in  $t + \theta \Delta t$ , i.e.,  $\sigma_{i+1} = \sigma_i + \theta \Delta \sigma_{i+1}$ .  $\theta$  is taken between  $[0, 1]$ , in this case, the implementation is fully implicit ( $\theta = 1$ ). As a function  $f$  of strain increments, the implicit equations associated to the state variables are given by:

$$f \epsilon^{el} = \Delta \epsilon^{el} - \Delta \epsilon^{to} + \Delta \epsilon^{kv} + \Delta \epsilon^{dash} \quad (11a)$$



$$f\epsilon^{kv} = \Delta\epsilon^{kv} - \frac{\Delta t}{\tau_v} \left[ q_{kv} \mathbb{C}_v : \sigma|_{t+\theta\Delta t} - \epsilon^{kv}|_{t+\theta\Delta t} \right] \quad (11b)$$

$$f\epsilon^{dash} = \Delta\epsilon^{dash} - \frac{\Delta t}{\eta_{dash}} \mathbb{C}_v : \sigma|_{t+\theta\Delta t} \quad (11c)$$

Finally, these equations are solved by a Newton-type optimization method. The solving algorithm is presented in [42] and comprises several steps:

1. For a given time  $t$  in between  $t_i$  and  $t_{i+1} = t_i + \Delta t_{i+1}$ ,  $\Delta\epsilon_{i+1}$  is known. At the beginning of the time step, the elastic stress increment is computed:

$$\Delta\sigma_{i+1} = \mathbb{K} : \Delta\epsilon_{i+1} \quad (12)$$

with  $\mathbb{K}$  the fourth order elastic tensor explicitly given in Appendix B.

2. With this first estimation of the stress increment  $\Delta\sigma_{i+1}$ , the Newton minimization starts. The effective stress  $\bar{\sigma}$  is computed (Equation (7)) at  $t + \theta\Delta t$ .
3. Nonlinear parameters are computed according to Equations (6a) and (6b).
4. The new increment  $\Delta\sigma_{i+1}$  which minimizes the implicit system constituted by Equations (11a), (11b) and (11c) is determined.
5. If the minimization criterion is reached with the computed stress increment, then the minimization process stops, otherwise it returns to stage 2.
6.  $i$  is incremented and the process goes to stage 1.

### 2.2.2. Implementation with MFront

The nonlinear creep model has been implemented using MFront tool (version 3.0) [42]. A Newton–Raphson algorithm with a numerical Jacobian made it possible to solve the system of nonlinear equation. Key implementation steps are summarized as follows:

1. At the beginning of the time step, the nonlinear parameters ( $\eta_{kv}$ ,  $\eta_{dash}$  and  $E_{kv}$ ) are computed on each Gauss point.
2. Then, one must find the stress increment  $\Delta\sigma$  which verifies the structural equilibrium for a given strain increment  $\Delta\epsilon$  from the incremental relationship given in the Section 2.2.1.
3. Once the equilibrium is reached, the variables  $\sigma_{i+1}$ ,  $\epsilon_{i+1}^{el}$  and  $\epsilon_{i+1}^v$  are updated.

## 3. Practical Case Studies

### 3.1. Samples of Bulk Epoxy Adhesive Subjected to Uniaxial Creep Loading

In a first stage, the constitutive law developed in the present work is compared with experimental data from a previous study [17], in which samples of bulk epoxy adhesive (Sikadur 30<sup>®</sup> from Sika Company) were subjected to sustained tensile loading. In this work, compliance master curves were constructed from series of a thermally stimulated tests according to the TTSP method. These master curves made it possible to obtain reference creep curves of the bulk epoxy adhesive over a 30-day period and for three load levels (i.e., at 5, 8 and 10 MPa). As the stress state is considered homogeneous within the sample, the problem can be simulated on a Gauss point in 0D, or alternatively on a unit cube. In this context, numerical simulations can be performed using Mtest module in 0D [42,43], or with the combined application of MFront and Code\_Aster to an elementary FE cube (eight nodes, four Gauss points). A creep period of 30 days was considered in the simulations to facilitate comparison with experimental results. The input values of the model parameters were determined as follows: tensile tests were carried to evaluate the elastic modulus of the epoxy adhesive ( $E_k$ ) [17], providing a mean value of 12.7 GPa very close to that reported in the technical data sheet [45]. A value of 0.3 was taken for the Poisson's ratio  $\nu$  of the epoxy adhesive in the vitreous state, as generally reported in the literature. The other model parameters were numerically identified from experimental data (Figure 2) and are reported in Table 1.



**Table 1.** Identified set of parameters of the proposed nonlinear creep model, for the bulk epoxy adhesive, subjected to sustained tensile loading.

$E_{kv}^0$ (GPa)	$a_{kv}$ (MPa <sup>-1</sup> )	$\eta_{kv}^0$ (GPa s)	$b_{kv}$ (MPa <sup>-1</sup> )	$\eta_{dash}^0$ (GPa s)	$b_{dash}$ (MPa <sup>-1</sup> )
10.8	$-1.10 \times 10^{-1}$	$3.47 \times 10^5$	$-1.19 \times 10^{-1}$	$2.88 \times 10^8$	$-3.14 \times 10^{-1}$

Simulations provided by the two modelling methods (use of Mtest or combination of MFfront-Code\_Aster) are found consistent and are also fitting very well the experimental evidences (Figure 2). Moreover, in their work, Houhou et al. [17] fitted the creep master curves obtained at various stress levels using a linear Burgers rheological model, and then interpolated the variations of the model parameters over the stress range to manage the nonlinearities. The nonlinear functions developed in the present work are found to match very well with the parameter interpolations reported by Houhou et al. (Figure 3). These results support the validity of the nonlinear functions assumed in the present approach.

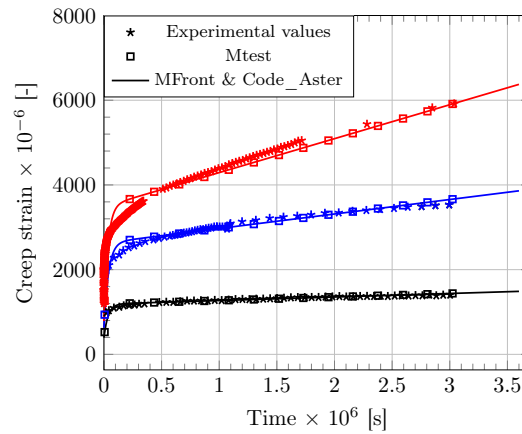


**Figure 2.** Comparison between theoretical and experimental strain for the bulk epoxy adhesive submitted to tensile creep at 5 MPa (black), 8 MPa (blue) and 10 MPa (red).

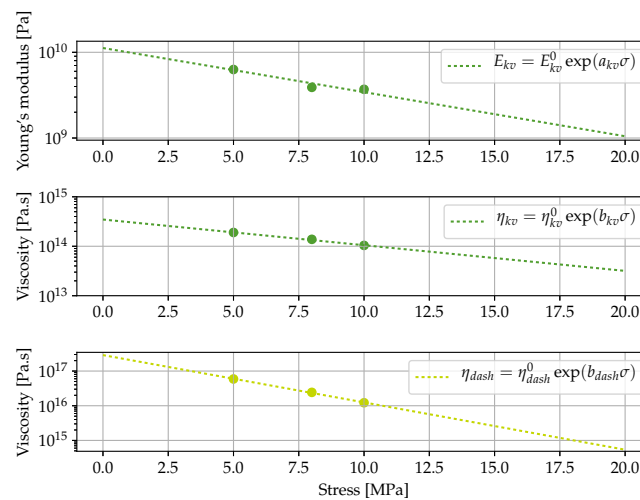


**Figure 3.** Comparison between the nonlinear functions identified in the present approach and the linear Burgers' parameters identified at different stress levels by Houhou et al. [17].

### 3.2. Structural Modelling

#### 3.2.1. Experimental Setup

The second application is concerned with the modelling of a creep test on a double shear specimen previously developed by Houhou et al. [17,45]. The setup consists of two concrete blocks of dimensions  $205 \times 210 \times 320 \text{ mm}^3$ , connected by two CFRP (carbon fiber reinforced polymer) plates which are bonded to the lateral faces with the Sikadur 30 adhesive (here after referred to as “Face 1” and “Face 2”, see Figure 4). To ensure a perfect adhesion between composite plates and concrete, a specific surface treatment was applied. A step of abrasion with a grinding machine was performed to increase concrete’s roughness. In addition, CFRP plates were carefully degreased using a specific solvent. The mechanical loading was applied through a flat hydraulic jack installed at the center of the specimen, which pushes the concrete blocks and exerts a shear load on the concrete–CFRP joint. The hydraulic pressure was adjusted to provide an average shear stress of 0.6 MPa in the adhesive joints, which corresponds to 30% of the bond strength at 25 °C. This pressure was then maintained at a constant level during the entire creep test, thanks to a 10-liter accumulator connected to the hydraulic loop. In addition, the CFRP plates were instrumented by five strain gages bonded at their top surface (Figure 4). These sensors allow to evaluate the strain distribution along the adhesive joint, just after loading and during the creep phase as well. This creep experiment was conducted over one month. More details regarding this experimental setup can be found in [17,45].

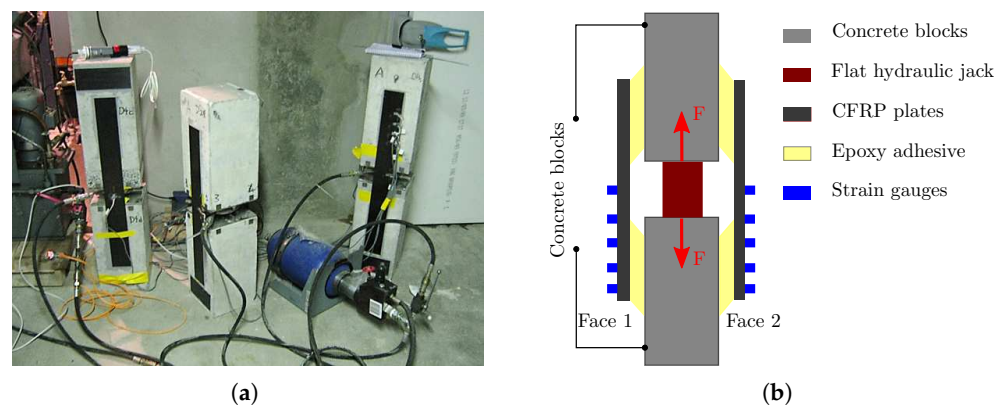


**Figure 4.** Creep test setup on double shear specimen previously proposed by Houhou et al. [17,45]. (a) Picture of the experimental setup, (b) principle of the test and loading procedure.

#### 3.2.2. Description of the FE Model

Due to the symmetry of the system (geometry and boundary conditions), only one eighth of the system is modelled (Figure 5a shows the boundary conditions). The FE mesh (Figure 5b) consists of 10189 linear hexahedrons. All component materials are assumed to exhibit a linear elastic behavior, except the epoxy adhesive. This assumption is motivated by the negligible creep response of the CFRP laminate in the longitudinal direction [46] and the low level of stress in concrete member (around 0.6 MPa). The CFRP composite is 1.2 mm thick and has an elastic modulus of 165 GPa and a Poisson’s ratio of 0.3. For the concrete material, values of 35 GPa and 0.3 were taken as the elastic modulus and the Poisson’s ratio, respectively. In the mesh, the adhesive joint is 1 mm thick and is represented by five layers of elements. Perfect bond is assumed between the different layers of concrete, adhesive and CFRP. Boundary conditions are imposed according to the scheme displayed (Figure 5a) and the sustained load is directly imposed on the cross section of the CFRP plate. Simulations were conducted considering a creep period of 30 days and different mechanical behaviors of the adhesive layer (i.e., elastic behavior, linear and nonlinear creep behaviors). Input parameters related to the adhesive layer that were implemented in the FE model are those previously reported in Table 1. In the case of an elastic behavior, only

the parameter  $E_k$  was considered and the others were set to zero. To describe linear creep, parameters  $a_{kv}$ ,  $b_{kv}$ ,  $b_{dash}$  were taken equal to zero, whereas the whole set of parameters was implemented in the case of a nonlinear creep behavior.

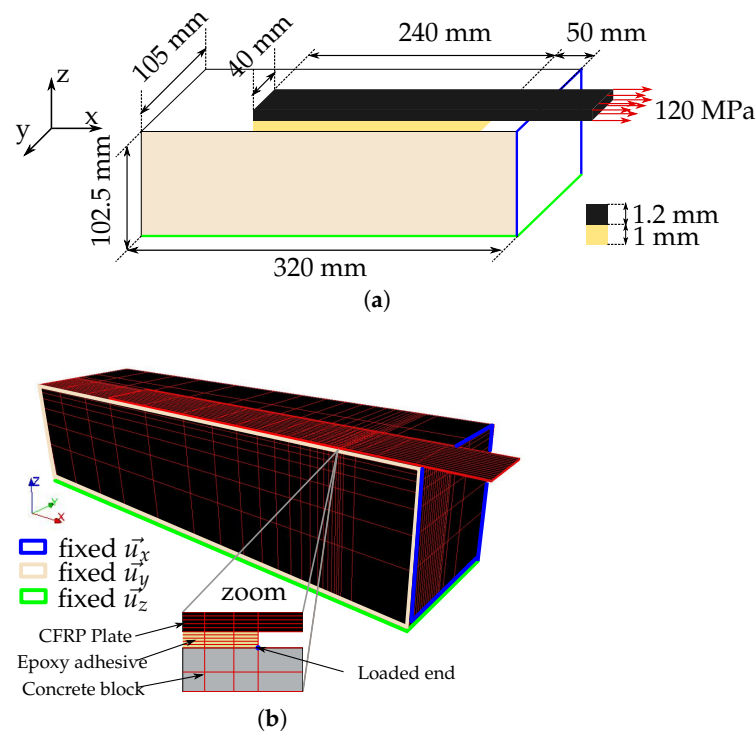


**Figure 5.** (a) Schematic representation and mesh of the double shear test, (b) associated FE mesh in Code\_Aster.

### 3.2.3. Confrontation between FE Model and Experimental Results

Figure 6 shows the strain profiles along the adhesive joint after the initial load application (Figure 6a) and after one month creep (Figure 6b). Both experimental data collected by the strain gages and theoretical profiles provided by the FE model are displayed in the graphs. Simulations are found globally consistent with the experimental evidences: strain values are around  $600 \times 10^{-6}$  at the loaded edge of the adhesive joint and fall to zero at 140 mm far from the edge.

However, the elastic and linear creep models tend to underestimate the strain values along the adhesive joint, both on the instantaneous and delayed responses. Differently, the nonlinear creep model captures well the strain profile from the loaded edge of the joint to a distance of 40–60 mm away from the edge, and then slightly underestimate the strain values over this distance. This can be explained both by the non-identification of the parameters on this experimental setup and by the model assumptions.

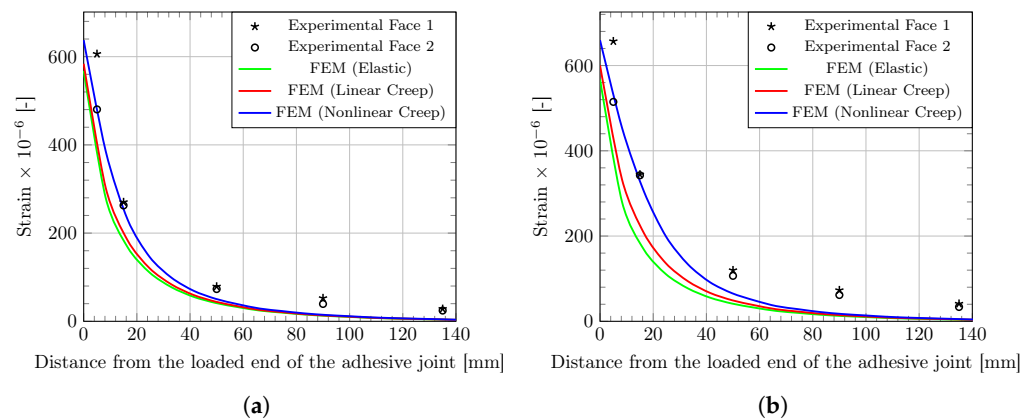


**Figure 6.** Axial strain ( $\epsilon_{xx}$ ) profiles along FRP–concrete adhesive joint, (a) after the loading stage and (b) after an one-month creep period. Experimental data and simulations provided by the FE model considering different behaviors of the adhesive layer.

The modelling of adhesive shear creep was conducted using a creep model calibrated on tensile creep experiments. This simplified approach previously used by other authors [17,29] was adopted in the present work because experimental data of tensile creep tests performed on the same adhesive material were readily available from previous work (see Section 3.1). This attempt to model the shear creep behaviour of adhesive with such an assumption seems to be validated, in view of the good agreement between the simulations and the experimental data. In a further study, a more robust approach may be to calibrate the model directly from shear creep test data to capture the actual shear creep behaviour of the polymer adhesive. However, in practice, the implementation of these tests is more difficult than the creep test in tensile configuration.

#### 3.2.4. Sensitivity Analysis of the Elastic Parameters

To assess the influence of the properties of each component material (concrete, CFRP, adhesive) on the strain response of the bonded assembly, the effect of a finite variation in the Young's modulus ( $E_i$ ) of each component on strain profiles along the bonded joint is computed using the elastic FE model. The sensitivity of the strain profile to variations of 10% in the Young's moduli of the various component materials is displayed in Figure 7. A variation in the stiffness of the CFRP material affects the strain profile over few millimeters near the loaded end and its influence decreases rapidly with the distance from the joint edge. In the same way, the strain profile is highly affected by a variation in stiffness of the epoxy adhesive near the joint edge, but the influence of the concrete's modulus becomes predominant beyond a distance of 40–60 mm. This predominance may explain the gap between theoretical results and experimental data. In this study, there is no concern about concrete variability and concrete creep is neglected. These two assumptions may be the root of the differences.

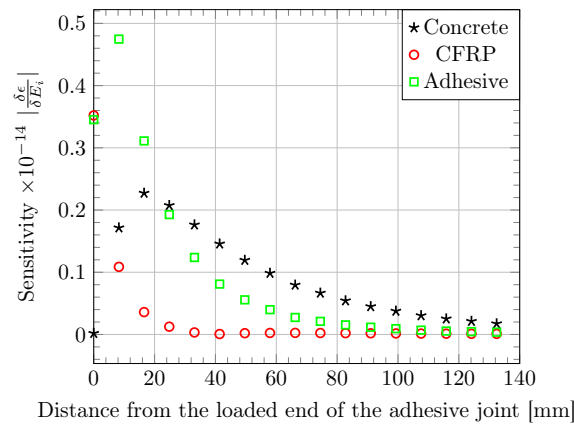


**Figure 7.** Sensitivity of the strain profile along the bonded joint to a 10% variation in the elastic moduli of the component materials, as evaluated using the elastic FE model.

### 3.2.5. Impact of Adhesive Creep on Stress Transfer Process

Finally, to investigate deeper the effect of creep on the load transfer process between the CFRP laminate and the concrete support, an analysis of the tangential stress distribution along the bonded joint (i.e., shear stress  $\tau(x)$ ) was carried-out. Tangential stresses were determined from experimental strain data, according to the procedure detailed in [17]. This method considers the equilibrium of an infinitesimal section of CFRP. As the distance between two strain gages is small, tangential stress is assumed constant over this length noted  $dx$ . Finally, a combination of the equilibrium equation and Hooke’s law makes it possible to express tangential stress versus strain (see Equation (13)).

$$\left. \begin{aligned} \tau(x)dx &= -e_{cp}d\sigma \\ d\sigma &= E_{cp}d\epsilon \end{aligned} \right\} \Rightarrow \tau(x) = -e_{cp}E_{cp} \frac{d\epsilon}{dx} \tag{13}$$

with  $e_{cp}$  (m) and  $E_{cp}$  (Pa) the thickness and the Young’s modulus of the CFRP composite, respectively. Distribution of tangential stress along the lap joint determined by this method is plotted in Figure 8 (experimental data), together with the simulations provided by the FE model considering different types of behavior for the adhesive layer. As expected, stress distributions resulting from these various configurations are rather different. When examining the peak shear stress near the joint edge, values of 17.0, 11.8 and 5.50 MPa are obtained for the elastic, linear creep and nonlinear creep models, respectively.

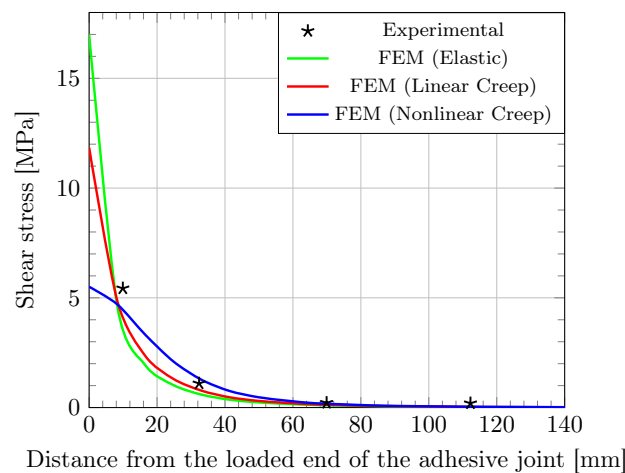


**Figure 8.** Shear stress profile along the bonded joint after a creep period of 30 days. Experimental data and simulations provided by the FE model considering different behaviors of the adhesive layer.

As previously noticed for the strain distribution, the elastic FE model, that reflects the instantaneous behavior, is not able to capture the actual stress distribution and overestimate the peak value. In other words, it appears that creep induces a stress relaxation near the loaded end as previously reported by other researchers [15,31]. Differently, the stress profile predicted by the nonlinear creep model seems more coherent with experimental data, especially near the joint edge.

In addition, the anchorage length (which corresponds to the segment of the joint bearing at least 97% of the load applied to the assembly, according to Yuan [47]) estimated from the nonlinear creep simulation seems consistent with that from experimental data. As reported by others authors [18], the anchorage length is increased by the creep phenomenon.

#### 4. Conclusions

This study has proposed a numerical investigation of the shear creep behavior of adhesive joints in the case of concrete structures reinforced by externally bonded CFRPs. This behavior is of particular importance near the loaded edge of the joint which is subjected to stress concentrations. In a first stage, constitutive equations were established using fully-3D formulation in order to describe the nonlinear creep response of the bulk adhesive. They were implemented using MFront tool and following an implicit method. The model parameters were identified by fitting creep strain data of bulk epoxy specimens which were available from a previous study. A FE model was then constructed by introducing the constitutive law in Code\_Aster. In order to validate this numerical model, simulations were carried out according to the double shear creep test configuration proposed by Houhou et al. [17]. A good agreement was found with experimental evidence.

In addition, another interesting point revealed by those simulations is that the creep phenomenon occurring within the polymer adhesive modifies the stress distribution in the bonded joint and mitigates stress concentrations near the loaded edge (in comparison with the stress profile provided by a pure elastic model). This effect seems more effective when considering a nonlinear creep behavior of the polymer adhesive rather than a linear behavior. Furthermore, the simulations suggests that creep leads to an increased transfer length. This feature should be taken into account in the design of bonded FRP reinforcements. Finally, to further investigate the ageing behavior and the creep of adhesive joints, it may be interesting to refine the proposed model by taking into account the impact of environmental conditions such as temperature, relative humidity and material ageing in the modelling process. Furthermore, most of time, externally bonded systems are applied after several years of service and concrete has already experienced most part of its creep potential (basic creep or drying creep). Nonetheless, it may be interesting to consider concrete creep in the modelling in order to improve the robustness of theoretical outcomes.

**Author Contributions:** Conceptualization, F.S., M.Q. and K.B.; Methodology, F.S., M.Q. and K.B.; Formal analysis, F.S., M.Q. and K.B.; Investigation, F.S.; Writing—original draft, F.S.; Writing—review & editing, F.S., M.Q. and K.B.; Project administration, K.B. All authors have read and agreed to the published version of the manuscript.

**Funding:** This research received no external funding.

**Institutional Review Board Statement:** Not applicable.

**Informed Consent Statement:** Not applicable.

**Data Availability Statement:** Data available on request.

**Conflicts of Interest:** The authors declare no conflict of interest.

#### Abbreviations

The following abbreviations are used in this manuscript:

EB	Externally Bonded
FE	Finite Element
FRP	Fiber Reinforced Polymer
RC	Reinforced Concrete
TTSP	Time Temperature Superposition Principle

### Appendix A. Unit Tensor of Elastic Compliance

$$\mathbb{C}_v = \begin{pmatrix} 1 & -\nu & -\nu & 0 & 0 & 0 \\ -\nu & 1 & -\nu & 0 & 0 & 0 \\ -\nu & -\nu & 1 & 0 & 0 & 0 \\ 0 & 0 & 0 & (1+\nu) & 0 & 0 \\ 0 & 0 & 0 & 0 & (1+\nu) & 0 \\ 0 & 0 & 0 & 0 & 0 & (1+\nu) \end{pmatrix} \quad (\text{A1})$$

with  $\nu$  (-) the elastic Poisson's coefficient.

### Appendix B. Unit Tensor of Elastic Stiffness

$$\mathbb{K} = \begin{pmatrix} 2\mu + \lambda & \lambda & \lambda & 0 & 0 & 0 \\ \lambda & 2\mu + \lambda & \lambda & 0 & 0 & 0 \\ \lambda & \lambda & 2\mu + \lambda & 0 & 0 & 0 \\ 0 & 0 & 0 & 2\mu & 0 & 0 \\ 0 & 0 & 0 & 0 & 2\mu & 0 \\ 0 & 0 & 0 & 0 & 0 & 2\mu \end{pmatrix} \quad (\text{A2})$$

with  $\lambda$  (Pa) and  $\mu$  (Pa) the Lamé's coefficients.

## References

- Nanni, A.; Dolan, C. *Fibre-Reinforced-Plastic (FRP) Reinforcement for Concrete Structures: Properties and Application; Developments in Civil Engineering*; Elsevier: Amsterdam, The Netherlands, 1993.
- Karbhari, V.M.; Seible, F. Fiber Reinforced composites—advanced materials for the renewal of civil infrastructure. *Appl. Compos. Mater.* **2000**, *7*, 95–124. [\[CrossRef\]](#)
- Smith, S.T.; Teng, J. FRP-strengthened RC beams I: Review of debonding strength models. *Eng. Struct.* **2002**, *24*, 385–395. [\[CrossRef\]](#)
- Wu, H.C.; Eamon, C.D. *Strengthening of Concrete Structures Using Fiber Reinforced Polymers (FRP): Design, Construction and Practical Applications*; Elsevier: Amsterdam, The Netherlands, 2017.
- Al-Mahaidi, R.; Kalfat, R. *Rehabilitation of Concrete Structures with Fiber-Reinforced Polymer*; Butterworth-Heinemann: Oxford, UK, 2018.
- Fayyadh, M.M.; Razak, H.A. Externally bonded FRP applications in RC structures: A state-of-the-art review. *Jordan J. Civ. Eng.* **2021**, *15*, 157–179.
- Japan Society of Civil Engineers (JSCE). *Recommendations for Upgrading of Concrete Structures with Use of Continuous Fiber Sheet*; Concrete Engineering Series (41); Japan Society of Civil Engineers: Tokyo, Japan, 2001.
- ACI Committee 440. *Guide for the Design and Construction of Externally Bonded FRP Systems for Strengthening Concrete Structures*; 440.2R-17; ACI: Farmington Hills, MI, USA, 2017.
- ISIS Canada Corporation. *FRP Rehabilitation of Reinforced Concrete Structures*; ISIS Design Manual No. 4; ISIS Canada Corporation: Winnipeg, MB, Canada, 2008.
- CNR—Advisory Committee on Technical Recommendations for Construction. *Guide for the Design and Construction of Externally Bonded FRP Systems for Strengthening Existing Structures*; National Research Council: Rome, Italy, 2013.
- Association Française de Génie Civil (AFGC). *Seismic Retrofitting of Reinforced Concrete Structures Using Composites: Temporary Recommendations*; AFGC: Paris, France, 2015.
- Fib Bulletin 90. *Externally Applied FRP Reinforcement for Concrete Structures*; The International Federation for Structural Concrete (Fib): Lausanne, Switzerland, 2019.
- Mazzotti, C.; Savoia, M. Stress redistribution along the interface between concrete and FRP subject to long-term loading. *Adv. Struct. Eng.* **2009**, *12*, 651–661. [\[CrossRef\]](#)
- Hamed, H.; Bradford, M. Flexural time-dependent cracking and post-cracking behavior of FRP strengthened concrete beams. *Int. J. Solids Struct.* **2012**, *49*, 1595–1607. [\[CrossRef\]](#)
- Hamed, E.; Chang, Z.T. Effect of creep on the edge debonding failure of FRP strengthened RC beams—A theoretical and experimental study. *Compos. Sci. Technol.* **2013**, *74*, 186–193. [\[CrossRef\]](#)



16. Houachine, H.R.E.; Sereir, Z.; Amziane, S. Creep model for the long-term behaviour of combined cohesive-bridging model of FRP-concrete interface debonding under axial loading. *Eur. J. Environ. Civ. Eng.* **2021**, *26*, 5594–5616. [[CrossRef](#)]
17. Houhou, N.; Benzarti, K.; Quiertant, M.; Chataigner, S.; Fléty, A.; Marty, C. Analysis of the nonlinear creep behavior of concrete/FRP-bonded assemblies. *J. Adhes. Sci. Technol.* **2014**, *28*, 1345–1366. [[CrossRef](#)]
18. Benzarti, K.; Chataigner, S.; Quiertant, M.; Marty, C.; Aubagnac, C. Accelerated ageing behaviour of the adhesive bond between concrete specimens and CFRP overlays. *Constr. Build. Mater.* **2011**, *25*, 523–538. [[CrossRef](#)]
19. Diab, H.; Wu, Z.; Iwashita, K. Short and long-term bond performance of prestressed FRP sheet anchorages. *Eng. Struct.* **2009**, *31*, 1241–1249. [[CrossRef](#)]
20. Fischer, J.; Bradler, P.R.; Schmidtbauer, D.; Lang, R.W.; Wan-Wendner, R. Long-term creep behavior of resin-based polymers in the construction industry. *Mater. Today Commun.* **2019**, *18*, 60–65. [[CrossRef](#)]
21. Silva, P.; Valente, T.; Azenha, M.; Sena-Cruz, J.; Barros, J. Viscoelastic response of an epoxy adhesive for construction since its early ages: Experiments and modelling. *Compos. Part B Eng.* **2017**, *116*, 266–277. [[CrossRef](#)]
22. Emara, M.; Torres, L.; Baena, M.; Barris, C.; Moawad, M. Effect of sustained loading and environmental conditions on the creep behavior of an epoxy adhesive for concrete structures strengthened with CFRP laminates. *Compos. Part B* **2017**, *129*, 88–96. [[CrossRef](#)]
23. Gómez, J.; Barris, C.; Jahani, Y.; Marta, B.; Torres, L. Experimental study and numerical prediction of the bond response of NSM CFRP laminates in RC elements under sustained loading. *Constr. Build. Mater.* **2021**, *288*, 123082. [[CrossRef](#)]
24. Bradler, P.; Fischer, J.; Wan-Wendner, R.; Lang, R. Shear test equipment for testing various polymeric materials by using standardized multipurpose specimens with minor adaptations. *Polym. Test.* **2019**, *75*, 93–98. [[CrossRef](#)]
25. Brinson, H. The viscoelastic constitutive modelling of adhesives. *Composites* **1982**, *13*, 377–382. [[CrossRef](#)]
26. Zanni-Deffarges, M.; Shanahan, M. Diffusion of water into an epoxy adhesive: Comparison between bulk behaviour and adhesive joints. *Int. J. Adhes. Adhes.* **1995**, *15*, 137–142. [[CrossRef](#)]
27. Ferrier, E.; Michel, L.; Jurkiewicz, B.; Hamelin, P. Creep behavior of adhesives used for external FRP strengthening of RC structures. *Constr. Build. Mater.* **2011**, *25*, 461–467. [[CrossRef](#)]
28. Jeong, Y.; Lopez, M.; Bakis, C. Effects of temperature and sustained loading on the mechanical response of CFRP bonded to concrete. *Constr. Build. Mater.* **2016**, *124*, 442–452. [[CrossRef](#)]
29. Zehsaz, M.; Vakili-Tahami, F.; Saeimi-Sadigh, M.A. Parametric study of the creep failure of double lap adhesively bonded joints. *Mater. Des.* **2014**, *64*, 520–526. [[CrossRef](#)]
30. Hadjazi, K.; Sereir, Z.; Amziane, S. Creep response of intermediate flexural cracking behavior of reinforced concrete beam strengthened with an externally bonded FRP plate. *Int. J. Solids Struct.* **2016**, *94–95*, 196–205. [[CrossRef](#)]
31. Hamed, E.; Bradford, M.A. Creep in concrete beams strengthened with composite materials. *Eur. J. Mech. A/Solids* **2010**, *29*, 951–965. [[CrossRef](#)]
32. European Committee for Standardisation (CEN). *Eurocode 2: Design of Concrete Structures—Part 1-1: General Rules and Rules for Buildings (EN 1992-1-1:2004)*; European Committee for Standardisation: Brussels, Belgium, 2004.
33. Bouziadi, F.; Boulekbache, B.; Haddi, A.; Hamrat, M.; Djelal, C. Finite element modeling of creep behavior of FRP-externally strengthened reinforced concrete beams. *Eng. Struct.* **2020**, *204*, 109908. [[CrossRef](#)]
34. Akpınar, S.; Aydin, M.D.; Özel, A. A study on 3-D stress distributions in the bi-adhesively bonded T-joints. *Appl. Math. Model.* **2013**, *37*, 10220–10230. [[CrossRef](#)]
35. Houhou, N.; Benzarti, K.; Quiertant, M.; Chataigner, S.; Youssef, G.; Rabasse, M.; Aubagnac, C.; Gagnon, A.; Fléty, A. Durability of concrete/FRP bonded assemblies subjected to hydrothermal coupled creep ageing mechanisms: Experimental and numerical investigations. In Proceedings of the TRA 2014, Paris, France, 14–17 April 2014; p. 10.
36. Wineman, A.S.; Rajagopal, K.R. *Mechanical Response of Polymers: An Introduction*; Cambridge University Press: Cambridge, UK, 2000.
37. Jiang, S.; Yao, W.; Jin, C.; Cai, T. Finite Element Modeling of FRP-Strengthened RC Beam under Sustained Load. *Adv. Mater. Sci. Eng.* **2018**, *45*, 1368–1376. [[CrossRef](#)]
38. Findley, W.N.; Laiand, J.S.; Onaran, K.; Christensen, R.M. Creep and relaxation of nonlinear viscoelastic materials. *J. Appl. Mech.* **1977**, *44*, 364. [[CrossRef](#)]
39. Dean, G. Modelling non-linear creep behaviour of an epoxy adhesive. *Int. J. Adhes. Adhes.* **2007**, *27*, 636–646. [[CrossRef](#)]
40. Tervoort, T.; Klompen, E.; Govaert, L. A multi-mode approach to finite, three-dimensional, nonlinear viscoelastic behavior of polymer glasses. *J. Rheol.* **1996**, *40*, 779–797. [[CrossRef](#)]
41. Majda, P.; Skrodziewicz, J. A modified creep model of epoxy adhesive at ambient temperature. *Int. J. Adhes. Adhes.* **2009**, *29*, 396–404. [[CrossRef](#)]
42. Helfer, T.; Michel, B.; Proix, J.M.; Salvo, M.; Sercombe, J.; Casella, M. Introducing the open-source mfront code generator: Application to mechanical behaviours and material knowledge management within the PLEIADES fuel element modelling platform. *Comput. Math. Appl.* **2015**, *70*, 994–1023. [[CrossRef](#)]
43. Helfer, T.; Fandeur, O.; Haboussa, D.; Deloison, D.; Jamond, O.; Munier, R.; Berthon, L.; CASTELIER, E.; Ramière, I. New functionalities of the 3.0 version of TFEL, MFront and MTest. In Proceedings of the 13e Colloque National en Calcul des Structures, Université Paris-Saclay, Giens, France, 14–19 September 2017.
44. CEA and EDF. MFront Web Site. Available online: <http://www.tfel.sourceforge.net> (accessed on 11 January 2023).

45. Houhou, N. Durabilité des Interfaces Collées Béton/Renforts Composites: Développement d'une Méthodologie D'étude basée sur un Dispositif de Fluage Innovant Conçu pour être Couplé à un Vieillissement Hygrothermique. Ph.D. Thesis, Université Paris-Est, Créteil, France, 2012.
46. Ascione, F.; Berardi, V.; Feo, L.; Giordano, A. An experimental study on the long-term behavior of CFRP pultruded laminates suitable to concrete structures rehabilitation. *Compos. Part B Eng.* **2008**, *39*, 1147–1150. [[CrossRef](#)]
47. Yuan, H. Improved theoretical solutions of FRP-to-concrete interfaces. In Proceedings of the International Symposium on Bond Behaviour of FRP in Structures, BBFS, Hong Kong, China, 7–9 December 2005; pp. 97–102.

**Disclaimer/Publisher's Note:** The statements, opinions and data contained in all publications are solely those of the individual author(s) and contributor(s) and not of MDPI and/or the editor(s). MDPI and/or the editor(s) disclaim responsibility for any injury to people or property resulting from any ideas, methods, instructions or products referred to in the content.